Tunable Programmable Microwave Photonic Filters Based on an Optical Frequency Comb

Ehsan Hamidi, *Student Member, IEEE*, Daniel E. Leaird, *Senior Member, IEEE*, and Andrew M. Weiner, *Fellow, IEEE*

***Abstract*—We demonstrate the application of optical combs to implement tunable programmable microwave photonic filters. We design well-known multi-tap microwave photonic filters; however, the utilization of an optical comb with a dispersive medium enables scaling of these filters to a large number of taps. We use optical line-by-line pulse shaping to program tap weights, which allows us to shape the filter's bandpass. Our scheme is simple and easily implementable, which provides filters with arbitrary tap weights. As an example, we implement filters with Gaussian apodized tap weights, which achieve more than 35-dB sidelobe suppression. Our experiments provide usable bandwidth, free of sampling spurs, over a Nyquist zone of 5 GHz, equal to half of our 10-GHz comb repetition frequency. Furthermore, we introduce a simple new technique, based on a programmable optical delay line, to uniformly tune the passband center frequency across the free spectral range (FSR) of the filter, ideally without changing the bandpass shape. We demonstrate this scheme by tuning the filter over a full FSR, equal to 10.4 GHz in our experiments.**

***Index Terms*—Finite impulse response filters, microwave photonics, optical combs, optical processing, programmable filters, tunable filters.**

I. Introduction

MICROWAVE photonics has been investigated for the past three decades to enhance radio frequency (RF) systems performance. In early years, microwave photonics focused on delay lines [1], followed by microwave photonic filters [2][3]–[13], and finally with microwave photonic waveform generators [14]–[18]. The idea of microwave photonic filters is based on optical processing of wideband analog RF signals. As Fig. 1 depicts, the RF signal is modulated onto an optical signal and processing of the signal takes place in the optical domain, followed by optical to electrical conversion [2]. The complexity of the implemented filters depends on the complexity of the optical processing.

In contrast to recent work on microwave photonic filters based on Fourier transform optical pulse shaping [5], most microwave photonic filters are based on the multi-tap delay line concept. The multi-tap delay line concept is the basis of two most common categories of microwave photonic filters. In the first scheme, the RF signal is modulated onto an optical source and then demultiplexed into a number of physical optical delay lines. The outputs are multiplexed together and fed into a photodiode to convert the optical signal to an electrical signal. In order to have a configuration free from environmental effects and thus stable and repeatable performance, the source coherence time is chosen much smaller than the differential delay between taps, resulting in an incoherent regime in which the photodetector output is the sum of the optical powers of the filter samples [2]. Although the shape of the filter transfer function can be programmed by adjusting the tap weights, generally the bandpass peak is set by the differential delay between taps and may not be tuned. In the second scheme, which has been explored more recently, the optical source comprises multiple optical frequencies which are modulated and passed through a dispersive medium. Because the dispersion introduces a differential delay between optical frequencies, the multiple optical frequencies act as multiple taps. The multiple frequency source has been implemented by using a mode-locked laser [6], by combining a few continuous-wave (CW) sources [7]–[10], or a spectrally sliced broadband source [11], [12]. Due to cost, it is difficult to reach a large number of taps by combining CW lasers. Slicing the spectrum of a broadband source was proposed in [11] and [12] to resolve this problem; however, this technique still does not a provide means to tune the filter.

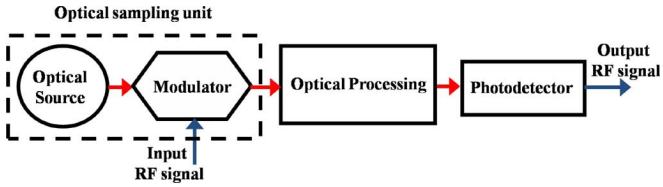

Fig. 1. Photonic processing of analog RF signals.

Much effort has been made in the past couple of years to implement tunable filters free of baseband response [6]–[11]. Some of these techniques have been based on adjusting the filter free spectral range (FSR) to achieve tunability; however, these schemes still suffer from the baseband response, and filter tuning alters the bandpass shape [6]. Some other techniques can achieve tunability without the baseband response, but their tunability is in discrete steps [7]. Techniques based on stimulated Brillouin scattering can obtain complex tap coefficients, resulting in tuning. However, such schemes are complicated by the need to generate multiple interacting optical waves and require rather high optical powers to pump the nonlinear interaction [8]. Most recently, a narrowband optical filter implemented by a phase-shifted fiber Bragg grating has been used to impose

Manuscript received January 06, 2010; revised August 02, 2010; accepted August 15, 2010. Date of publication October 18, 2010; date of current version November 12, 2010. This work was supported by the Naval Research Laboratory/Defense Advanced Research Projects Agency under Grant N00173-090-1-G904 and by the Naval Postgraduate School under Grant N00244-09-1-0068 under the National Security Science and Engineering Faculty Fellowship program.

The authors are with the School of Electrical and Computer Engineering, Purdue University, West Lafayette, IN 47907-2035 USA (e-mail: ehamidi@purdue.edu; leaird@purdue.edu; amw@purdue.edu).

Color versions of one or more of the figures in this paper are available online at http://ieeexplore.ieee.org.

Digital Object Identifier 10.1109/TMTT.2010.2076970

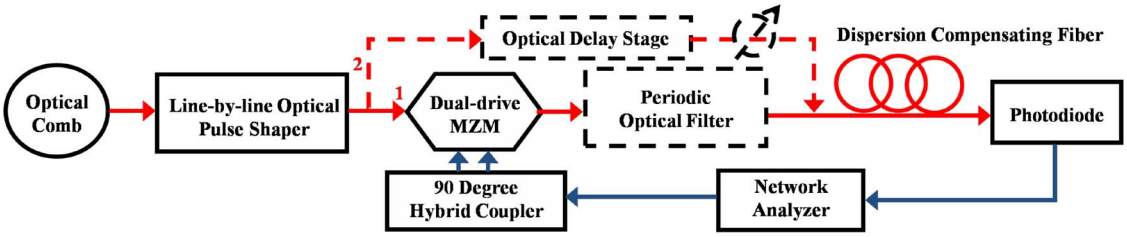

Fig. 2. Configuration of tunable programmable microwave photonic filter. The dashed lines shows portions included only in our second scheme.

a variable phase on the optical carrier with respect to the sideband by controlling the carrier frequency [9], or cross-polarization of the sideband and the carrier has been used to impose a programmable phase on the sideband by a spatial light modulator [10]. Thus far, these schemes have not been shown to scale to a substantial number of filter taps.

Here, for the first time to our knowledge, we demonstrate microwave photonic filtering based on an optical comb source and a dispersive medium. Essentially, an optical comb consists of an evenly spaced set of narrow linewidth optical tones, in which both the frequency spacing and the absolute frequencies remain approximately constant. By using an optical comb, we are able to exploit line-by-line pulse shaping [19] to manipulate the intensities of individual frequency tones. This enables programmable apodization of the tap amplitudes, which allows us to achieve clean bandpass shapes with more than 35-dB sidelobe suppression.

Furthermore, we demonstrate a new scheme, based on passing the comb through an interferometer into which the modulator is embedded, that makes possible tuning of the RF passband frequency while maintaining independent programmable apodization capability. Both apodization and RF frequency tuning exploit the narrow optical linewidth, hence long coherence time, of optical comb sources, which is in sharp contrast to many traditional microwave photonic filtering approaches based on short coherence time sources. A summary of preliminary results obtained using this scheme was reported in [20]. Here, for the first time, we present a complete theoretical analysis, as well as substantially improved tuning results, including 12 dB higher tunable filter sidelobe suppression and tuning over most of ~10-GHz filter free spectral range.

It is also worth comparing our scheme with a different approach to programmable RF filtering previously demonstrated in our group [5]. In the previous scheme using a single continuous-wave laser, a hyperfine-resolution Fourier transform pulse shaper provides programmable optical filter functions which are mapped directly into the RF domain. In other words there is a direct mapping between the spectral amplitude response of the optical filter (with respect to the laser carrier frequency) and the spectral amplitude response of the resulting RF filter (referenced to baseband). However, in our current scheme, using a comb of optical frequencies, the shaped optical power spectrum is mapped into the time domain by utilizing a dispersive element; hence, the spectral response of the realized RF filter is related to the Fourier transform of a scaled optical filter function. The sidelobe suppression in [5] is limited by the line shape of the virtually imaged phased array device and the extinction of the spatial light modulator device used in the hyperfine pulse shaper. Here, the sidelobe suppression is limited primarily by the precision with which the optical spectrum is apodized. As a result, here we achieve 10 dB higher sidelobe suppression compared to [5].

II. Concept and Theory

Fig. 2 shows our experimental setup. An optical comb generated by a strongly phase modulated CW laser based on the technique shown in [21] is passed through a line-by-line pulse shaper in which we control the intensity of the comb lines. The optical line-by-line pulse shaper is based on Fourier transform pulse shaping [22]. Here, we pursue two related schemes: first, we demonstrate apodization (allowing control of the filter shape) and then tunability.

In the first approach, the components shown in dashed lines are not present. The comb through path 1 is single-sideband modulated in a dual-drive Mach–Zehnder (MZ) modulator biased at quadrature point (half power point or in other words at $V_\pi/2$) and driven by a pair of RF signals with 90° phase difference [23]. The modulator output is sent through a dispersive fiber. The output optical signal is detected using a photodiode and measured by a network analyzer.

We assume an optical comb consisting of N lines and write its electric field as

$$e(t) \propto \sum_{n=0}^{N-1} \sqrt{p_n} e^{j(\omega_n t+\phi_n)} + \text{c.c.} \tag{1}$$

where p_n, ω_n, and ϕ_n are the optical intensity, angular frequency, and phase of the nth line, respectively, and c.c. stands for the complex conjugate of the first term on the right side. For a comb, the optical frequencies satisfy $\omega_n = \omega_0 + n\Delta\omega$, and the intensity of the comb source is periodic at repetition frequency $\Delta\omega$. Later, we will see through derivations that the initial phases of the lines do not affect the RF filter function, which is also verified by an experiment. The RF electrical signal is split into two equal RF signals with 90° phase difference using a broadband 90° hybrid splitter. The RF outputs are applied to the two arms of the MZ modulator. Each of the comb lines undergoes a single sideband modulation [23]. The output electric field corresponding to the nth line can be written as

$$e_n(t) \propto \sqrt{p_n} \left\{ e^{j\left[\omega_n t+\phi_n-\frac{\pi}{2}+\pi\frac{v_{\mathrm{RF}}}{\sqrt{2}V_\pi}\cos(\omega_{\mathrm{RF}}t)\right]} + e^{j\left[\omega_n t+\phi_n+\pi\frac{v_{\mathrm{RF}}}{\sqrt{2}V_\pi}\sin(\omega_{\mathrm{RF}}t)\right]} \right\} + \text{c.c.} \tag{2}$$

where v_{RF} is the voltage amplitude of driving RF signal into 90° hybrid splitter, and V_π is the half-wave voltage of the MZ modulator. Assuming $\pi v_{\mathrm{RF}} \ll \sqrt{2}V_\pi$, we can approximate (2) as

$$e_n(t) \propto \sqrt{p_n} e^{j(\omega_n t+\phi_n)} \left[e^{-j\frac{\pi}{4}} + \frac{\pi v_{\mathrm{RF}}}{2V_\pi} e^{j\omega_{\mathrm{RF}} t} \right] + \text{c.c.} \quad (3)$$

where the first term in brackets is the output optical carrier, and the second term is the higher frequency sideband generated at $\omega_n + \omega_{\mathrm{RF}}$. After propagation through a dispersive medium, the electric field can be written as

$$e_n(t) \propto \sqrt{p_n} e^{j(\omega_n t+\phi_n)} \times \left[e^{j\left[-\frac{\pi}{4}+\psi(\omega_n)\right]} + \frac{\pi v_{\mathrm{RF}}}{2V_\pi} e^{j[\omega_{\mathrm{RF}} t+\psi(\omega_n+\omega_{\mathrm{RF}})]} \right] + \text{c.c.} \quad (4)$$

where $\psi(\omega)$ is the quadratic phase introduced by the chromatic dispersion [23] given by

$$\psi(\omega) = -\beta(\omega)L = \psi_0 + \psi_1(\omega-\omega_0) + \frac{\psi_2}{2}(\omega-\omega_0)^2 \quad (5)$$

where the coefficient ψ_2 relates to the dispersion parameter D (in ps/nm/km) as

$$\psi_2 = -\beta_2 L = \frac{D\lambda^2 L}{2\pi\, c}. \quad (6)$$

At the photodiode, the total optical electric field can be written as

$$\begin{aligned} e(t) &= \sum_{n=0}^{N-1} e_n(t) \\ &\propto \sum_{n=0}^{N-1} \sqrt{p_n} e^{j(\omega_n t+\phi_n)} \\ &\quad \times \left[e^{j\left[-\frac{\pi}{4}+\psi(\omega_n)\right]} + \frac{\pi v_{\mathrm{RF}}}{2V_\pi} e^{j[\omega_{\mathrm{RF}} t+\psi(\omega_n+\omega_{\mathrm{RF}})]} \right] + \text{c.c.} \end{aligned} \quad (7)$$

The photodiode output current is given by

$$i(t) \propto \frac{1}{2} k \left\langle |e(t)|^2 \right\rangle \quad (8)$$

where k is the responsivity of the photodiode, and $\langle\ \rangle$ stands for averaging over the optical oscillations [25].

After working out the math, we can see that $i(t)$ will have terms at frequencies of $m\Delta\omega$ and $m\Delta\omega \pm \omega_{\mathrm{RF}}$, where m is an integer. $m\Delta\omega$ are RF frequencies representing beating between comb lines, and $m\Delta\omega \pm \omega_{\mathrm{RF}}$ are RF frequencies representing beating between comb lines and sidebands. In order to operate the filter in a spur free regime (we have neglected the nonlinearity of the modulator by the approximation made in (3)), the usable frequency span should be limited to a single Nyquist zone, which runs from $m\Delta\omega/2$ through $(m+1)\Delta\omega/2$, where m is a nonnegative integer. We note that, in network analyzer measurements, these spurs do not appear. If desired, a low pass filter with a cut-off frequency of $\Delta\omega/2$ may be used to limit operation to the lowest Nyquist zone ($m = 0$). Alternately, a bandpass filter centered at frequency $(2m+1)\Delta\omega/4$ and bandwidth $\Delta\omega/2$ may be used to limit operation to a single Nyquist zone for $m \geq 1$.

After simplification, we can show that the component of the current with frequency ω_{RF} is given by

$$i_{\omega_{\mathrm{RF}}}(t) \propto \sum_{n=0}^{N-1} k p_n \frac{\pi v_{\mathrm{RF}}}{2V_\pi} e^{j[\omega_{\mathrm{RF}} t+\psi(\omega_n+\omega_{\mathrm{RF}})-\psi(\omega_n)]} + \text{c.c.} \quad (9)$$

By substituting in the quadratic phase from (5), we find

$$i_{\omega_{\mathrm{RF}}}(t) \propto \sum_{n=0}^{N-1} k p_n \frac{\pi v_{\mathrm{RF}}}{2V_\pi} \times e^{j\left(\omega_{\mathrm{RF}} t+\psi_1\omega_{\mathrm{RF}}+n\psi_2\Delta\omega\omega_{\mathrm{RF}}+\frac{\psi_2}{2}\omega_{\mathrm{RF}}^2\right)} + \text{c.c.} \quad (10)$$

Therefore, we can write the filter transfer function as

$$H(\omega_{\mathrm{RF}}) \propto e^{j\left(\psi_1\omega_{\mathrm{RF}}+\frac{\psi_2}{2}\omega_{\mathrm{RF}}^2\right)} \sum_{n=0}^{N-1} p_n e^{jn\psi_2\Delta\omega\omega_{\mathrm{RF}}}. \quad (11)$$

We notice that the filter spectral amplitude response is periodic in frequency with a free spectral range (FSR) of

$$\mathrm{FSR} = \frac{1}{\psi_2\Delta\omega} = \frac{1}{T} \quad (12)$$

where $T = \psi_2\Delta\omega$ is the differential delay between taps. By taking an inverse Fourier transform of (11), we can write the time domain response function as

$$h(t) \propto \sum_{n=0}^{N-1} p_n e^{-j\frac{(t+nT+\psi_1)^2}{2\psi_2}}. \quad (13)$$

We note that while ψ_2 is negative for a dispersion compensating fiber resulting in negative T, $-\psi_1$ is the total group delay of dispersive fiber and always large enough to guarantee that $h(t)$ satisfies causality. The response function is a scaled version of the comb spectrum, which is the consequence of frequency-to-time mapping in a dispersive medium. The response function written in (13) is valid, assuming operation within a single Nyquist zone. For $p_n \geq 0$, the filter bandpass is at m/T, where m is an integer. We can shape the filter function by apodizing the p_n's.

The microwave photonic filters that we implement are based on the concept of multi-tap delay line filters that can be modeled by finite-impulse-response (FIR) filters. These filters have been fully studied in digital signal processing as discrete-time finite response filters [26].

In our second scheme, all the components in Fig. 2 are present. The modulator output is connected to a periodic optical filter in which we suppress the comb lines and instead mostly transmit the sidebands. We implement this periodic filter by an interferometer with 100-ps relative delay, which has a transmission with periodic nulls in frequency. This device is commonly used for differential phase-shift keying (DPSK) demodulation at 10 Gb/s. We tune the interferometer so that its frequency nulls match the comb carrier frequencies. The unmodulated comb in path 2 is passed through a controllable optical delay stage. The two paths are coupled back together, and we align

their polarization by using a polarizer controller in one arm. In this scheme, we show how the bandpass location can be tuned by programming the optical delay.

In order to tune the filter in frequency, we need to apply a phase that increments linearly with tap number. This has been done in [8]–[10]; however, these techniques are complicated and limited to small number of taps. Here, we demonstrate a technique that is intuitive and simple to implement. For an equally spaced set of frequencies, as with an optical comb, a phase linearly incrementing with tap number corresponds to a linear delay. The RF signal generated at the photodiode is a result of beating between sidebands and their corresponding carriers. Therefore, applying a delay on sidebands or on carriers will result in the introduction of the desired linear phase into the taps.

Before modulating the optical comb with an RF signal, we split part of the comb and pass it through a delay line. The rest of the comb is single sideband modulated with carrier suppressed. This can be obtained by dual-parallel MZ modulators in a nested configuration, which is available commercially, or a dual-drive MZ modulator followed by a periodic optical filter to suppress the carriers [23]. Thus, by combining the output of the modulator and the delayed version of the comb with an aligned polarization, we can write the output electric field corresponding to the nth line as

$$e_n(t) \propto \sqrt{p_n}\left[e^{j(\omega_n t - n\Delta\omega\tau - \omega_0\tau + \phi_n)} + \gamma\frac{\pi v_{\mathrm{RF}}}{4V_\pi}e^{j[(\omega_n+\omega_{\mathrm{RF}})t+\phi_n]}\right] + \text{c.c.} \quad (14)$$

where τ is the amount of delay that the delayed path is delayed more than the modulated path, γ^2 is the ratio of the modulated path intensity to the delayed path intensity after the final optical coupler. Here, we assumed that the carriers are ideally suppressed in single sideband carrier suppressed modulation. After propagation through a dispersive fiber, the electric field can be written as

$$e_n(t) \propto \sqrt{p_n}\left[e^{j[\omega_n t - n\Delta\omega\tau - \omega_0\tau + \psi(\omega_n) + \phi_n]} + \gamma\frac{\pi v_{\mathrm{RF}}}{4V_\pi}e^{j(\omega_n+\omega_{\mathrm{RF}})t+\psi(\omega_n+\omega_{\mathrm{RF}})+\phi_n}\right] + \text{c.c.} \quad (15)$$

Similarly we can show that the filter transfer function will be given by

$$H(\omega_{\mathrm{RF}}) \propto e^{j\left(\omega_0\tau+\psi_1\omega_{\mathrm{RF}}+\frac{\psi_2}{2}\omega_{\mathrm{RF}}^2\right)}\sum_{n=0}^{N-1} p_n e^{jn\Delta\omega(\psi_2\omega_{\mathrm{RF}}+\tau)}. \quad (16)$$

The most important point is that the transfer function can be tuned in the frequency domain by controlling τ the relative delay between two paths. The RF frequency shift is given by

$$\Delta f = -\frac{\tau}{2\pi\psi_2}. \quad (17)$$

Therefore, a programmable tuning can be achieved by a programmable optical delay stage. We also note, although the optical phase shift referenced to the carrier frequency $\omega_0\tau$ is transferred directly into the RF domain, it does not affect tuning of the filter. That is, the spectral amplitude response of the filter in (16) is independent of this phase.

From a practical point of view, obtaining a single sideband carrier suppressed modulation is a difficult task. Errors in fabrication of dual-parallel MZ modulators, imbalance of the RF signals' strength, and imbalance of 90° hybrid splitter result in non-deal operation and presence of residual carrier after modulation. Also, the thermal drift and sensitivity to biasing voltages lead us to a controlling circuitry with a feedback loop for biasing the modulator. Here, we briefly explain what will happen in the presence of residual carrier. The beat between the sidebands from modulated path and the carriers through the delayed path will result in a tunable filter as (16), but also the beat between the sidebands and the carriers through the modulated path results in a nontunable filter, which is given by (11). By neglecting the common multiplicative spectral phase factor preceding the summation sign in (11) and (16), we can write the overall filter frequency response as

$$H(\omega_{\mathrm{RF}}) \propto \gamma\sum_{n=0}^{N-1} p_n e^{-jn\psi_2\Delta\omega\omega_{\mathrm{RF}}} + e^{j\omega_0\tau}\sum_{n=0}^{N-1} p_n e^{-jn\Delta\omega(\psi_2\omega_{\mathrm{RF}}+\tau)}. \quad (18)$$

We point out a few assumptions that we have made in our analysis above. First, we have assumed the coherence time of individual optical comb lines is large compared to the small delay between modulated and delayed paths. This is easily satisfied for practical comb sources. Note, however, that spectral sliced amplified spontaneous emission (ASE) sources, used in [11], for example, do not meet this coherence time criterion and cannot be employed in our scheme. Also, we assume that the polarizations are aligned and that there are negligible polarization rotation fluctuations. Finally, note that when the intensity in the modulated path is much less than the intensity in the delayed path, in other words, for small values of γ, we can ignore the first term on the right side of (18), and it will be simplified to (16).

Here, we briefly explain what coupling ratio should be chosen for the optical splitter and coupler in our scheme. For the given optical power input to the splitter, we can show that the desired RF signal with a frequency of ω_{RF} (or, in other words, the filter transfer function) generated at the photodiode is also proportional to

$$H(\omega_{\mathrm{RF}}) \propto \sqrt{\alpha(1-\alpha)\beta(1-\beta)} \quad (19)$$

where α and β are the splitter and coupler coupling coefficients in terms of power. As we can see, the above expression is maximized when α and β are chosen equal to 0.5, or in other words, we choose 3-dB splitter and couplers.

We note that the DPSK demodulator interferometer that we use for carrier suppression also alters the frequency response of our implemented filters; however, this change is irrelevant when a single sideband carrier suppressed modulation is used.

The filter transfer function in presence of DPSK demodulator interferometer is given by

$$H(\omega_{\mathrm{RF}}) \propto \sqrt{\frac{\varepsilon-1}{2}\cos\left(2\pi\frac{\omega_{\mathrm{RF}}}{\Delta\omega}\right)+\frac{\varepsilon+1}{2}} \times\left[\sqrt{\varepsilon}\sum_{n=0}^{N-1}p_n e^{-jn\psi_2\Delta\omega\omega_{\mathrm{RF}}} +e^{j\omega_0\tau}\sum_{n=0}^{N-1}p_n e^{-jn\Delta\omega(\psi_2\omega_{\mathrm{RF}}+\tau)}\right] \quad (20)$$

where ε is the ratio of the nulls' amplitude to the peaks' amplitude of demodulator interferometer in terms of power transmission, or in other words $-10\log_{10}\varepsilon(\mathrm{dB})$ is the degree of extinction with which the demodulator interferometer suppress the carriers. Here, we assumed a 3-dB splitter and coupler. For small values of ε, the first term in brackets on the right side vanishes, and (19) will simplify as

$$H(\omega_{\mathrm{RF}}) \propto e^{j\omega_0\tau}\sin\left(\pi\frac{\omega_{\mathrm{RF}}}{\Delta\omega}\right)\sum_{n=0}^{N-1}p_n e^{-jn\Delta\omega(\psi_2\omega_{\mathrm{RF}}+\tau)}. \quad (21)$$

III. Experiment

A. Filter Programming

Here, we demonstrate the first approach in Fig. 2 to shape the filter bandpass using apodization of the comb. We use a 90° hybrid splitter with a bandwidth of 1–12.4 GHz and a phase imbalance of ±7°. A CW laser with 1-kHz linewidth is sent through a phase modulator driven at 20 GHz, followed by an intensity modulator driven at 10 GHz to generate an optical comb [21]. A dual-drive MZ modulator with a half-wave voltage of 4.5 V at 1 kHz and a 3-dB optical bandwidth of 12.2 GHz is used. Unless otherwise noted, we use a dispersion-compensating fiber with a specified chromatic dispersion of −1259.54 ps/nm at 1550 nm and relative dispersion slope (the ratio of dispersion slope to dispersion at 1550 nm) of 0.00455/nm, resulting in a delay difference of 96 ps between adjacent 10-GHz-spaced comb lines (taps). The photodiode has a 3-dB bandwidth of 22 GHz with a responsivity of 0.6 A/W. We measure the filter transfer functions using a network analyzer over a span of 300 kHz–20 GHz.

In order to compare our experimental results with simulation, we make some assumptions. We run our simulations based on (11); however, this relation does not include some of the factors affecting the overall frequency response of our filter. The cable loss, the modulator transfer function, and the photodiode response are all frequency dependent and roll off for higher frequencies. Since we do not have an accurate measure of all these frequency responses, we introduce a way to subtract these effects from experimental results, so that we end up with plots that can be compared with simulation results. In order to measure the frequency roll-offs, we remove the dispersive fiber from our setup and connect the output of modulator directly to the photodiode. Thus, we do not have the filtering response due to tapped delay lines. Then, we measure the transfer function and also record the optical power measured at the photodiode. Fig. 3 shows the filter transfer function, plotted in RF gain units, when we remove the dispersion compensating fiber and the optical power into the photodiode is about 5.5 dBm. Although Fig. 3 is measured using the optical comb source, a similar curve is obtained using the CW laser directly provided that the optical power is held constant. Most of the roll-off up to ∼12 GHz arises from the frequency response of the modulator (since 3-dB optical bandwidth of the modulator translates into a 6-dB drop in the RF gain). The measured transfer function includes all the losses and roll-offs. In comparing our experimental results with simulation, we subtract this transfer function from our measured filter transfer functions while correcting for optical power applied to the photodiode.

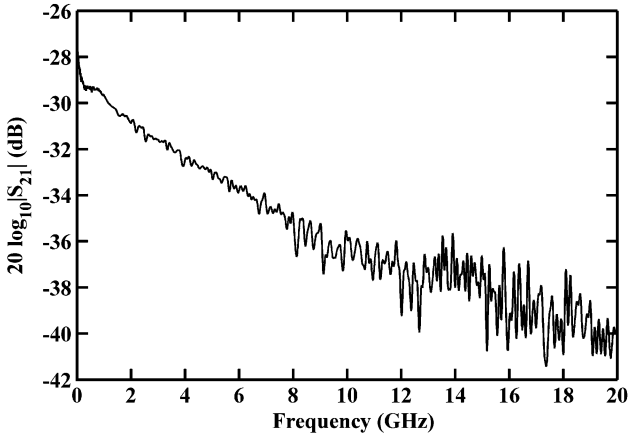

Fig. 3. The link frequency response without the dispersion compensating fiber.

Fig. 4(a) shows the optical comb at the photodiode when there is no programming applied to the spatial light modulator in the line-by-line pulse shaper. As we notice, the comb is not uniform, and the intensity of the lines has a large variation from one to the other. This is a characteristic common to many comb sources, such as ours [21], based on strong periodic phase modulation of a continuous-wave source. Fig. 4(b) shows the normalized filter transfer function as a solid line, and the simulated filter transfer function as a dashed line. The filter has a 3-dB bandwidth of ∼510 MHz, and the main sidelobe suppression is 9 dB. The location of the filter bandpass gives us the FSR of filter, which is 10.4 GHz, which is in accord with the 96-ps tap delay. As we see, there is a close agreement between simulated and measured filter functions. The vertical dashed lines separate the Nyquist zones; the filter can be used in a regime free of sampling spurs over the span of any one of these zones. This statement also holds for following plots in Figs. 5(b), 6(a), 6(b), 7(b), 7(c), 8(b), and 8(c).

Next, we apodize the optical comb with a Gaussian apodization, which is shown in Fig. 5(a) using the line-by-line pulse shaper. Due to the Fourier transform property of the Gaussian function, we expect the filter transfer function also to have a Gaussian profile in which the sidelobes are highly suppressed. Fig. 5(b) shows the normalized filter transfer function as a solid line, and the simulated filter transfer function as a dashed line. As we see, there is a close agreement between simulated and measured filter functions. The filter has a 3-dB bandwidth of

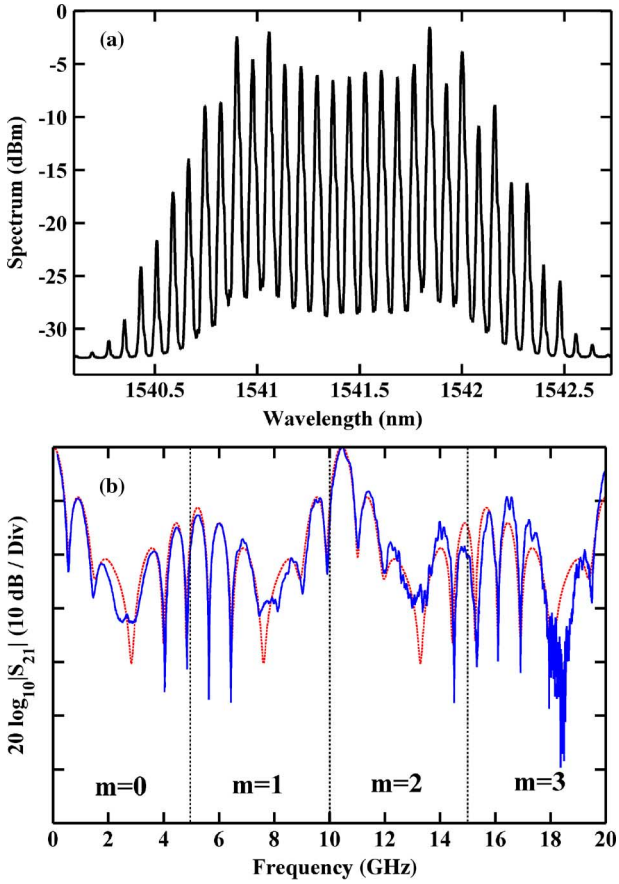

Fig. 4. (a) Non-apodized optical comb. (b) Normalized (blue) and simulated (red) filter transfer functions. The vertical dashed lines depict individual Nyquist zones, where m refers to the zone number, explained earlier in the text. The filter can be used in a spur free regime within the span of any one of these zones.

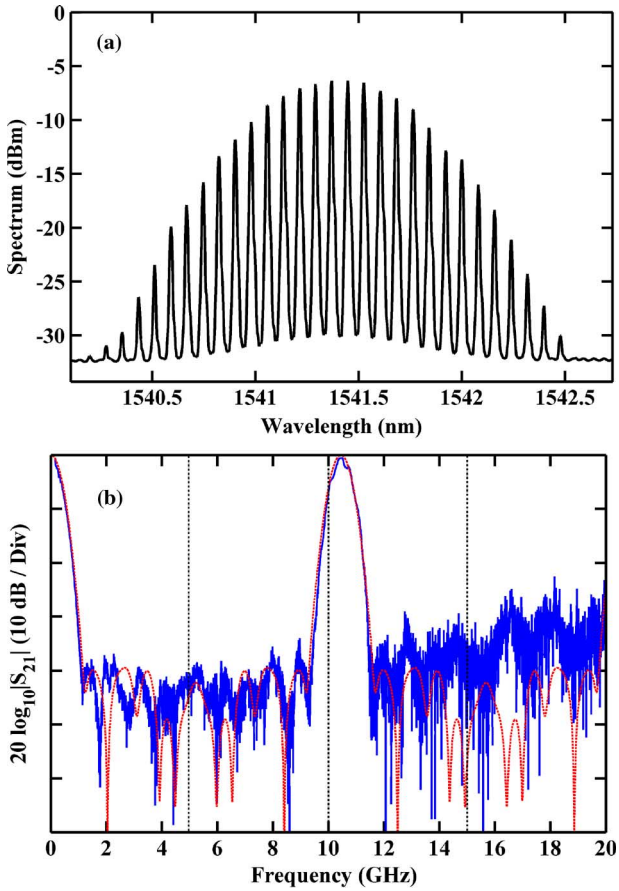

Fig. 5. (a) Gaussian apodized optical comb. (b) Normalized (blue) and simulated (red) filter transfer functions.

$\sim$630 MHz, and the sidelobes between 1–12 GHz are suppressed by more than 35 dB and close to 40 dB, in agreement with the simulation. We attribute the higher noise levels for frequencies above $\sim$12 GHz both to our normalization process, in which the negative slope plot in Fig. 3 is subtracted from the experimental results, and to the higher noise floor of our network analyzer above 10 GHz.

The improvement of the apodized filter compared to the unapodized case is striking. Note, however, that although the comb in Fig. 5(a) has been apodized for a target Gaussian profile, the actual profile has small deviations compared to an ideal Gaussian. Fig. 5(a) deviates from a quadratic profile by 0.37 dB in terms of root mean square. According to our MATLAB simulations, the 30-line ideal Gaussian which is the best fit to our actual comb spectrum would exhibit a sidelobe suppression of more than 63 dB! Therefore, extremely clean filter shapes should be possible via our technique, although very accurate apodization will be essential for achieving the highest quality filters.

Here, we remind the reader that as we pointed out in Section II, a variety of tones, at frequencies $m\Delta\omega$ and $m\Delta\omega \pm \omega_{\mathrm{RF}}$, are present at the output of our filter. However, in a network analyzer measurement, which is based on coherent mixing with a reference tone, only a signal with frequency equal to that transmitted from the network analyzer is acquired. In other words, a network analyzer measures the scattering parameters that correspond to the linear response of filter. Mixing tones resulting from the periodic sampling process inherent in our optical comb based filter implementation are not recorded. We note that , due to the limited length of dispersion compensating fiber available, the filter bandpass in the experiments of Figs. 4 and 5 occurs at 10.4 GHz, close to the beat term at the comb repetition frequency ($\Delta f = 10$ GHz) as well as the sampling spur at frequency $2\Delta\omega - \omega_{\mathrm{RF}}$.

By using comb sources with larger repetition frequency, unwanted beat terms and spurs can be pushed to higher frequencies. Alternately, with increased dispersion, the bandpass can be shifted to lower frequency to avoid the beat terms. Fig. 6 shows normalized and simulated filter transfer functions for experiments in which we added additional DCF to increase the dispersion by about 32.5%. The filter bandpasses are shifted to 7.85 GHz, as expected, near the center of the $m = 1$ Nyquist zone. Therefore, if these filters are operated near their bandpasses, the nearest spurs will be a few gigahertz away. The filter corresponding to the unapodized comb has a 3–dB bandwidth of 394 MHz, and the main sidelobe suppression is 12.5 dB. The appearance is qualitatively similar to Fig. 4(b), although the details differ due to different details in the unapodized comb spectrum. The filter for Gaussian apodized comb has a 3-dB bandwidth of 567 MHz, with sidelobes between 1 and 12 GHz suppressed by more than 37 dB.

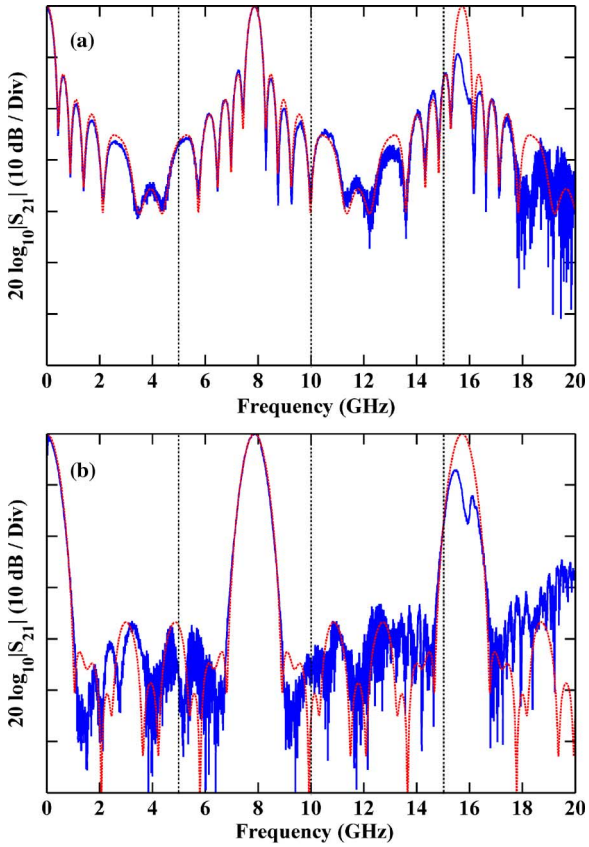

Fig. 6. (a) Normalized (blue) and simulated (red) filter transfer functions for unapodized comb. (b) Normalized (blue) and simulated (red) filter transfer functions for apodized comb.

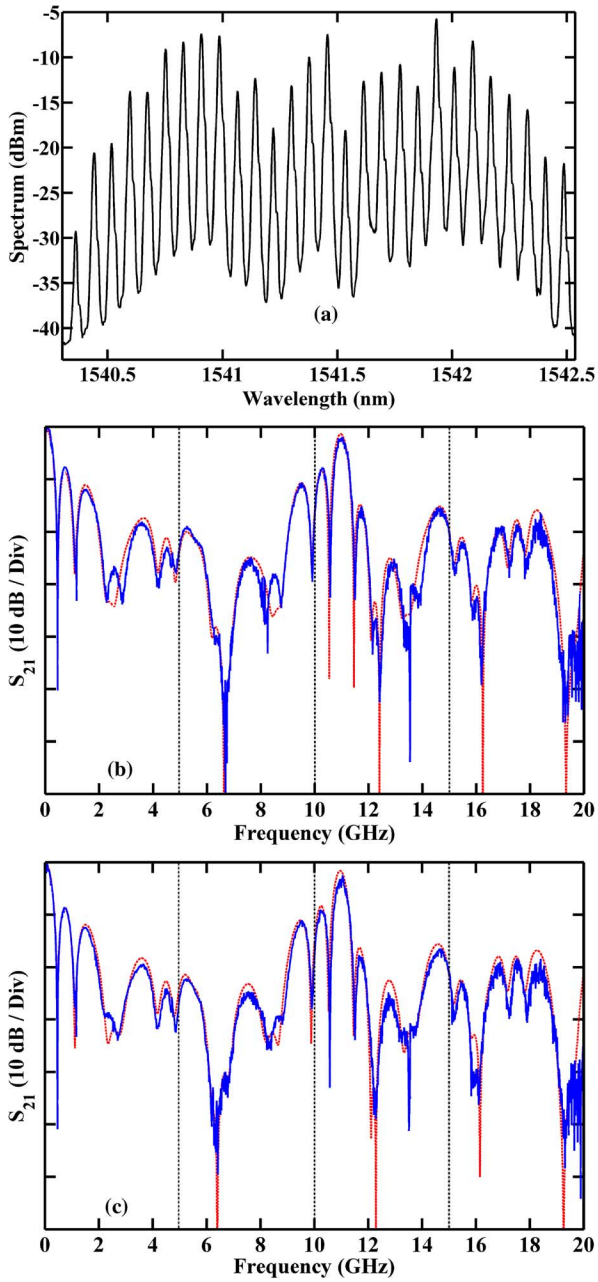

Fig. 7. (a) Optical comb. (b) Normalized (blue) and simulated (red) filter transfer functions for compensated comb. (c) Normalized (blue) and simulated (red) filter transfer functions for uncompensated comb.

It is also worth discussing the role of the phase of the optical comb lines out of the comb generator. Generally, the output of a comb generator such as ours, based on strong phase modulation of a CW laser, is NOT a train of bandwidth limited pulses. However, when desired, we can use the line-by-line pulse shaper to correct the phases of the comb lines, which does produce a train of bandwidth limited pulses (in other words, a phase-compensated comb) [21]. As predicted earlier by (11), the spectral phase of the optical comb source, ϕ_n, used as the sampling signal does not affect the RF filter response—a prediction that we now verify. Instead of the dual-drive MZ modulator depicted in Fig. 2, for this experiment, we used a standard Mach–Zehnder intensity modulator with a half-wave voltage of 4.75 V at 1 GHz and a 3-dB bandwidth of 35 GHz. Intensity modulation results in double sideband modulation rather than single sideband modulation. Also for this experiment, we employed a single-mode fiber with a length of about 70 km as the dispersive medium. No apodization is employed in these experiments.

Fig. 7(a) shows the optical comb measured at the photodiode. Fig. 7(b) shows the normalized and simulated transfer functions of the filter as solid and dashed lines respectively when the phases of the comb lines are compensated using the line-by-line pulse shaper. In this case we verified by intensity autocorrelation measurements that the comb consisted of a train of pulses, periodic at 10 GHz and with approximately bandwidth-limited pulse durations. This corresponds to at most linear phase across the comb lines. We note that, in this experiment, the filter frequency response is affected by the well-known frequency-dependent fading effect due to dispersion acting on double sidebands; this effect has been included in our simulation [27].

Fig. 7(c) shows the normalized and simulated transfer functions of the filter as solid and dashed lines, respectively, when the line-by-line pulse shaper is in a quiescent state; in other words, the phases of the comb lines are not compensated. Here the time-domain intensity profile of the comb source, although periodic, consists of only a weak modulation on a nearly constant background. The spectral phase, i.e., the comb line phases ϕ_n vary strongly from line to line. Measurements giving further details on the phases and temporal behavior of compensated and uncompensated combs may be found in [28] and [29]. The important point is that the data of Fig. 7(b) and 7(c) are nearly identical. This close agreement verifies our prediction that the

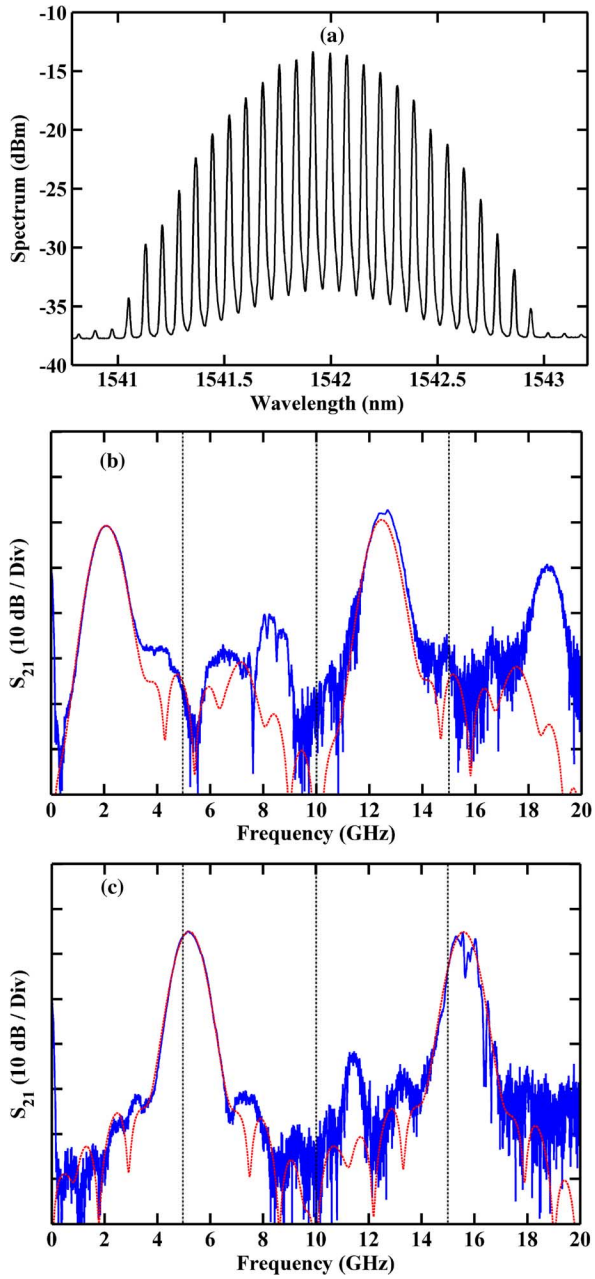

Fig. 8. (a) Gaussian apodized optical comb. (b) Normalized (blue) and simulated (red) filter transfer functions for m.100–20 ps relative delay. (c) Normalized (blue) and simulated (red) filter transfer functions for m.100–50 ps relative delay.

phases of the input comb lines do not influence the RF filter transfer function.

B. Filter Tuning

Now, in order to demonstrate filter tunability, we configure our setup as given by the second approach in Fig. 2. As we discussed earlier, we use a 3-dB splitter and coupler to obtain the minimum loss. To measure the Gaussian apodized optical comb at the photodiode, shown in Fig. 8(a), we disconnect the modulator path. The normalized filter transfer function is plotted in Fig. 8(b) in a solid line. The filter bandpass occurs at 2.1 GHz, which corresponds to a relative delay of m.100–20 ps, where m is an integer. We use (21) to simulate the filter transfer function, which is shown in Fig. 8(b) in a dashed line. In order to show tuning, we reduce the delay in the delayed path by 30 ps, and we measure the transfer function. We expect the filter bandpass shifts by 3.12 GHz to a higher frequency. Fig. 8(c) shows the normalized and simulated transfer functions in solid and dashed lines, respectively, where the bandpass occurs at 5.25 GHz. The frequency shift is very much as expected given the change in relative delay. The filter in Fig. 8(c) has a 3-dB bandwidth of $\sim$720 MHz and 36-dB sidelobe suppression over 0–10 GHz. These results confirm our prediction that filter tuning is possible, without baseband response and without significant change in passband width, by varying delay in an interferometric setup.

Compared to Fig. 5(b), Fig. 8(b) and (c) shows higher noise and some spurious peaks, which we discuss briefly in the following. First, we believe that the spurious peaks around 8.5 and 11.4 GHz in Fig. 8(b) and (c), respectively, arise due to undesired reflection in our setup. In effect, this could lead to an unwanted weak interference component with a different delay, corresponding to a different passband frequency. Therefore, for future experiments, care should be taken to reduce reflections, possibly taking advantage of optical isolators. On the other hand, the degradation of the 90° hybrid splitter above 12.4 GHz, not included in our simulations, results in unbalanced double sideband modulation, which can also produce undesired filter responses for frequencies above 12.4 GHz, to which we attribute the spurious peak at 18.7 GHz in Fig. 8(b). This is further investigated in [30].

Finally. we attribute the very weak peaks at 10.4 GHz in Fig. 8(b) and (c), which are more than 40 dB down compared to 5.25-GHz passband peak in Fig. 8(c), to finite extinction of the carrier in the modulator path. As in Fig. 5(b), any remaining carrier is expected to contribute a peak at the filter FSR, 10.4 GHz. We also notice from (21) that the use of a filter for carrier suppression in our tuning experiments of Fig. 8 leads to a $\sin(\pi\omega_{\mathrm{RF}}/\Delta\omega)$ frequency-dependent attenuation factor that is not present for the data of Fig. 5; this effect has been taken into account in our simulation.

Also as predicted in (19), for fixed input optical power, the interferometric filter configuration provides lower RF gain compared to the single path (noninterferometric) configuration. For a 3-dB splitter and coupler, the theoretical decrease in RF gain is 12 dB. Hence, we expect that our bandpass filter tuned to 5 GHz has 12 dB lower RF gain compared to Fig. 5(b). The bandpass filter at 5.25 GHz in Fig. 8(c) has 15 dB higher loss. which agrees closely since the DPSK demodulator interferometer has an additional insertion loss of about 2 dB. In the future, it should be possible to restore some of the reduced RF gain by using a complementary modulator configuration with differential detection [31].

Finally, we scan the delay stage in increments of 0.9375 mm (round trip delay of 6.25 ps) and measure the filter transfer function. The center of filter's bandpass as a function of the relative delay is plotted in Fig. 9. The solid circles show the measured filter's bandpass center, and the solid line shows a linear fit to the experimental results. The fit has a slope of 0.1025 GHz/ps. This corresponds to a 10.25-GHz frequency shift for a relative delay of 100 ps, which introduces a 2π incremental phase shift

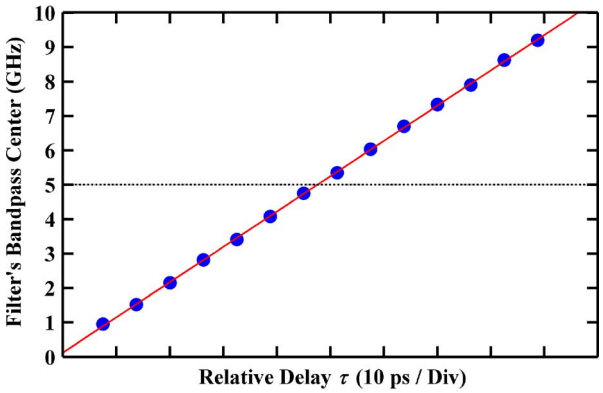

Fig. 9. Filter's bandpass center versus relative delay τ. The horizontal dashed line depicts the boundary between $m = 0$ and $m = 1$ Nyquist zones.

between adjacent taps; this closely agrees with the measured FSR of 10.4 GHz. The maximum deviation of the linear fit from the experimental results is 117 MHz. This clearly confirms the linear frequency tuning with respect to the programmable delay predicted by (17).

IV. Conclusion

We demonstrate a novel scheme based on optical frequency combs and dispersive propagation to implement microwave photonic filters scalable to large number of taps. By using line-by-line pulse shaping, we are able to individually program the tap weights in order to apodize the filter response and suppress the sidelobes. In the current experiments, we implemented filters composed of 30 comb lines apodized for a Gaussian profile, which enabled sidelobe suppression to below 35 dB. We also demonstrated a very simple technique to uniformly tune the filter bandpass across the filter free spectral range without altering the filter shape or the free spectral range and without introducing baseband response. With further development we believe it should be possible to implement filters with 100 taps or more and with even stronger sidelobe suppression.

Acknowledgment

The authors gratefully acknowledge helpful discussions with S. Tainta, J. D. McKinney, and R. Esman. The authors would also like to thank Prof. W. J. Chappell, Purdue University, West Lafayette, IN, for lending them a network analyzer at the start of this project.

References

[1] K. Wilner and A. P. Van Den Heuvel, "Fiber-optic delay lines for microwave signal processing," *Proc. IEEE*, vol. 64, no. 5, pp. 805–807, May 1976.

[2] J. Capmany, B. Ortega, D. Pastor, and S. Sales, "Discrete-time optical processing of microwave signals," *J. Lightw. Technol.*, vol. 23, no. 2, pp. 702–723, Feb. 2005.

[3] A. Seeds, "Microwave photonics," *IEEE Trans. Microw. Theory Tech.*, vol. 50, no. 3, pp. 877–887, Mar. 2002.

[4] R. A. Minasian, "Photonic signal processing of microwave signals," *IEEE Trans. Microw. Theory Tech.*, vol. 54, no. 2, pp. 832–846, Feb. 2006.

[5] S. Xiao and A. M. Weiner, "Coherent photonic processing of microwave signals using spatial light modulator: Programmable amplitude filters," *J. Lightw. Technol.*, vol. 24, no. 7, pp. 2523–2529, Jul. 2006.

[6] A. Ortigosa-Blanch, J. Mora, J. Capmany, B. Ortega, and D. Pastor, "Tunable radio-frequency photonic filter based on an actively mode-locked fiber laser," *Opt. Lett.*, vol. 31, no. 6, pp. 709–711, Mar. 2006.

[7] J. Mora, S. Sales, M. D. Manzanedo, R. Garcia-Olcina, J. Capmany, B. Ortega, and D. Pastor, "Continuous tuning of photonic transversal filter based on the modification of tapped weights," *IEEE Photon. Technol. Lett.*, vol. 18, no. 15, pp. 1594–1596, Aug. 2006.

[8] M. Sagues, A. Loayssa, and J. Capmany, "Multitap complex-coefficient incoherent microwave photonic filters based on stimulated Brillouin scattering," *IEEE Photon. Technol. Lett.*, vol. 19, no. 16, pp. 1194–1196, Aug. 2007.

[9] M. Sagues, R. G. Olcina, A. Loayssa, S. Sales, and J. Capmany, "Multi-tap complex-coefficient incoherent microwave photonic filters based on optical single-sideband modulation and narrow band optical filtering," *Opt. Exp.*, vol. 16, no. 1, pp. 295–303, Jan. 2008.

[10] T. Mengual, B. Vidal, and J. Marti, "Continuously tunable photonic microwave filter based on a spatial light modulator," *Opt. Commun.*, vol. 281, pp. 2746–2749, May 2008.

[11] J. H. Lee, Y. M. Chang, Y.-G. Han, S. B. Lee, and H. Y. Chung, "Fully reconfigurable photonic microwave transversal filter based on digital micromirror device and continuous-wave, incoherent supercontinuum source," *Appl. Opt.*, vol. 46, no. 22, pp. 5158–5167, Aug. 2007.

[12] J. Mora, L. R. Chen, and J. Capmany, "Single-bandpass microwave photonic filter with tuning and reconfiguration capabilities," *J. Lightw. Technol.*, vol. 26, no. 15, pp. 2663–2670, Aug. 2008.

[13] J. Mora, A. Ortigosa-Blanch, D. Pastor, and J. Capmany, "Tunable microwave photonic filter free from baseband and carrier suppression effect not requiring single sideband modulation using a Mach–Zehnder configuration," *Opt. Exp.*, vol. 14, no. 17, pp. 7960–7965, Aug. 2006.

[14] J. Chou, Y. Han, and B. Jalali, "Adaptive RF-photonic arbitrary waveform generator," *IEEE Photon. Technol. Lett.*, vol. 15, no. 4, pp. 581–583, Apr. 2003.

[15] I. S. Lin, J. D. McKinney, and A. M. Weiner, "Photonic synthesis of broadband microwave arbitrary waveforms applicable to ultrawideband communication," *IEEE Microw. Wireless Compon. Lett.*, vol. 15, no. 4, pp. 226–228, Apr. 2005.

[16] C. Wang and J. P. Yao, "Photonic generation of chirped millimeter-wave pulses based on nonlinear frequency-to-time mapping in a nonlinearly chirped fiber Bragg grating," *IEEE Trans. Microw. Theory Tech.*, vol. 56, no. 2, pp. 542–553, Feb. 2008.

[17] A. Zeitouny, S. Stepanov, O. Levinson, and M. Horowitz, "Optical generation of linearly chirped microwave pulses using fiber Bragg gratings," *IEEE Photon. Technol. Lett.*, vol. 17, no. 3, pp. 660–662, Mar. 2005.

[18] T. Yilmaz, C. M. DePriest, T. Turpin, J. H. Abeles, and P. J. Delfyett, "Toward a photonic arbitrary waveform generator using a modelocked external cavity semiconductor laser," *IEEE Photon. Technol. Lett.*, vol. 14, no. 11, pp. 1608–1610, Nov. 2002.

[19] Z. Jiang, C. B. Huang, D. E. Leaird, and A. M. Weiner, "Optical arbitrary waveform processing of more than 100 spectral comb lines," *Nature Photon.*, vol. 1, pp. 463–467, Aug. 2007.

[20] E. Hamidi, D. E. Leaird, and A. M. Weiner, "Microwave photonic filter based on optical comb and line-by-line optical pulse shaping," presented at the Conf. Lasers Electro-Optics, San Jose, CA, May 2010.

[21] C. B. Huang, S. G. Park, D. E. Leaird, and A. M. Weiner, "Nonlinearly broadened phase-modulated continuous-wave laser frequency combs characterized using DPSK decoding," *Opt. Exp.*, vol. 16, no. 4, pp. 2520–2527, Feb. 2008.

[22] A. M. Weiner, "Femtosecond pulse shaping using spatial light modulators," *Rev. Sci. Instrum.*, vol. 71, no. 5, pp. 1929–1960, May 2000.

[23] K. Takano, Y. Naganuma, and K. Nakagawa, "Performance analysis of optical single sideband modulation based on Mach–Zehnder interferometers and its dispersive fiber transmission," *IEICE Trans. Commun.*, vol. E88-B, no. 5, pp. 1994–2003, May 2005.

[24] A. M. Weiner, *Ultrafast Optics*, 1st ed. New York: Wiley, 2009.

[25] W. S. C. Chang, *RF Photonic Technology in Optical Fiber Links*, 1st ed. Cambridge, U.K.: Cambridge Univ. Press, 2002.

[26] A. V. Oppenheim and R. W. Schafer, *Discrete-Time Signal Processing*, 3rd ed. Englewood Cliffs, NJ: Prentice-Hall, 2009.

[27] F. Devaux, Y. Sorel, and J. F. Kerdiles, "Simple measurement of fiber dispersion and of chirp parameter of intensity modulated light emitter," *J. Lightw. Technol.*, vol. 11, no. 12, pp. 1937–1940, Dec. 1993.

[28] H. Miao, D. E. Leaird, C. Langrock, M. M. Fejer, and A. M. Weiner, "Optical arbitrary waveform characterization via dual-quadrature spectral shearing interferometry," *Opt. Exp.*, vol. 17, no. 5, pp. 3381–3389, Mar. 2009.
[29] V. R. Supradeepa, D. E. Leaird, and A. M. Weiner, "Optical arbitrary waveform characterization via dual-quadrature spectral interferometry," *Opt. Exp.*, vol. 17, no. 1, pp. 25–33, Jan. 2009.
[30] E. Hamidi, R. Wu, V. R. Supradeepa, C. M. Long, D. E. Leaird, and A. M. Weiner, "Tunable radio frequency photonic filter based on intensity modulation of optical combs," presented at the IEEE Int. Topical Meeting on Microwave Photonics, Montreal, QC, Canada, Oct. 2010.
[31] J. D. McKinney, M. Godinez, V. J. Urick, S. Thaniyavarn, W. Charczenko, and K. J. Williams, "Sub-10-dB noise figure in a multiple-GHz analog optical link," *IEEE Photon. Technol. Lett.*, vol. 19, no. 7, pp. 465–467, Apr. 2007.

Ehsan Hamidi (S'08) was born in Tehran, Iran, in 1983. He received the B.S. degree in electrical engineering from Sharif University of Technology, Tehran, Iran, in 2005 and the Ph.D. degree from Purdue University, West Lafayette, IN.

He has been a Research Assistant in the Ultrafast Optics and Optical Fiber Communications Laboratory in the School of Electrical and Computer Engineering, Purdue University, since 2005. His current research interests include radio frequency photonics, ultrafast optics, fiber optics, optical signal processing, optical frequency combs, and optical metrology.

Mr. Hamidi is a student member of the IEEE Lasers and Electro-Optics Society and the IEEE Communication Society. He was nominated as a student paper award finalist in Twenty-Ninth URSI General Assembly and the 2009 IEEE International Symposium on Antennas and Propagation. He has served as a reviewer for the IEEE/OSA JOURNAL OF LIGHTWAVE TECHNOLOGY, the IEEE PHOTONICS TECHNOLOGY LETTERS, *Optics Letters*, and *Optics Express*.

Daniel E. Leaird (M'01–SM'05) was born in Muncie, IN, in 1964. He received the B.S. degree in physics from Ball State University, Muncie, IN, in 1987 and the M.S. and Ph.D. degrees from the School of Electrical and Computer Engineering, Purdue University, West Lafayette, IN, in 1996 and 2000, respectively.

He joined Bellcore as a Senior Staff Technologist in 1987, and later advanced to Member of Technical Staff. From 1987 to 1994, he worked in the Ultrafast Optics and Optical Signal Processing Research Group, where he was a key team member in research projects in ultrafast optics, such as optical pulse shaping using liquid-crystal modulator arrays, investigation of dark soliton propagation in optical fibers, impulsive stimulated Raman scattering in molecular crystals, and all-optical switching. He is currently a Senior Research Scientist and Laboratory Manager of the Ultrafast Optics and Optical Fiber Communications Laboratory in the School of Electrical and Computer Engineering, Purdue University, where he has been since 1994. He has received several awards for his work in the ultrafast optics field, including a Bellcore Award of Excellence, a Magoon Award for outstanding teaching, and an Optical Society of America/New Focus Student Award. He has coauthored approximately 90 journal articles and 120 conference proceedings and has three issued U.S. patents.

Dr. Leaird is active in the optics community and professional organizations, including the Optical Society of America and the IEEE Photonics Society, where he served as the Chair of the Ultrafast Optics Technical Committee from 2006 to 2009. He has also served a consultant to venture capitalists by performing technical due diligence. He also serves as a frequent reviewer for *Optics Letters*, *Photonics Technology Letters*, *Applied Optics*, and the *Journal of the Optical Society of America B*, in addition to serving on the National Science Foundation review panels in the SBIR program.

Andrew M. Weiner (S'84–M'84–SM'91–F'95) graduated with the Sc.D. degree in electrical engineering from the Massachusetts Institute of Technology (MIT), Cambridge, in 1984.

Upon graduation, he joined Bellcore, first as Member of Technical Staff and later as Manager of Ultrafast Optics and Optical Signal Processing Research. In 1992, he joined Purdue University, West Lafayette, IN, where he is currently the Scifres Family Distinguished Professor of Electrical and Computer Engineering. His research focuses on ultrafast optics signal processing and applications to high-speed optical communications and ultrawideband wireless. He is especially well known for his pioneering work in the field of femtosecond pulse shaping using liquid-crystal modulator arrays.

Prof. Weiner has won numerous awards for his research, including the Hertz Foundation Doctoral Thesis Prize in 1984, the Adolph Lomb Medal of the Optical Society of America in 1990, the Curtis McGraw Research Award of the American Society of Engineering Education in 1997, the International Commission on Optics Prize in 1997, and the Alexander von Humboldt Foundation Research Award for Senior U.S. Scientists in 2000. He is joint recipient, with J.P. Heritage, of the IEEE LEOS William Streifer Scientific Achievement Award in 1999 and the OSA R. W. Wood Prize in 2008 and has been recognized by Purdue University with the inaugural Research Excellence Award from the Schools of Engineering in 2003 and with the Provost's Outstanding Graduate Student Mentor Award in 2008. He was named a U.S. Department of Defense National Security Science and Engineering Faculty Fellow in 2009. He is author of a textbook entitled *Ultrafast Optics* (Wiley, 2009), has published six book chapters and over 235 journal articles, and is holder of 12 U.S. patents. He is a Fellow of the Optical Society of America and is a member of the U.S. National Academy of Engineering. He has served as Co-Chair of the Conference on Lasers and Electro-Optics and the International Conference on Ultrafast Phenomena and as Associate Editor of several journals. He has also served as Secretary/Treasurer of IEEE LEOS and as a Vice-President of the International Commission on Optics (ICO). He is currently serving as Chair of the National Academy of Engineering's U.S. Frontiers of Engineering Meeting.